A&A 529, A51 (2011)
DOI: 10.1051/0004-6361/201016069

Astronomy & Astrophysics

The apparent "reversed" motion of gas and stars in M 82

A. Greve

Institut de Radio Astronomie Millimétrique, Domaine Universitaire, 38406 St. Martin d'Hères, France
e-mail: greve@iram.fr

Received 4 October 2010 / Accepted 27 January 2011

ABSTRACT

We summarize earlier and unpublished long-slit spectroscopic measurements of radial velocities of ionized gas and stars along and parallel to M 82's major axis to a radial distance of ~±2.5 kpc (~±140″) from the center. In the position-velocity diagram, these measurements indicate a velocity reversal of ~100 km s^{-1} of gas and/or stars at ~±1.0 kpc (~±50−70″) on either side of the center, outside the bar. Although seen in earlier observations, and perhaps neglected because they were assumed to be only an effect of heavy local extinction, the positional symmetry of the velocity reversal with respect to the center of M 82, as well as the absence of the reversal in the motion of stars seen in the near-IR Ca II absorption lines, points to another origin. M 82's two-armed spiral, as outlined by Mayya et al. (2005, ApJ, 628, L33), may explain a part of the velocity reversal, although this interpretation leaves inconsistencies so that other explanations must also be investigated. A simple, conclusive explanation of the velocity reversal has not yet been found. While restricted observationally in radial distance to ~120″ (2 kpc), the near-IR stellar Ca II absorption lines, which do not show the velocity reversal, indicate a flat radial velocity curve of the stellar disk that remained after the encounter with M 81.

Key words. galaxies: individual: M 82 – galaxies: kinematics and dynamics

1. Introduction

There is convincing observational evidence that an encounter occurred between M 81, M 82, and NGC 3077 several 100 Myr ago. The encounter has left long H I and CO tidal arms (Yun et al. 1993, 1994; Brouillet et al. 1991; Taylor et al. 2001; Walter et al. 2002). It reshuffled the stars and the gas of the original M 82-galaxy, formed a bar (Telesco et al. 1991; Larkin et al. 1994; Wills et al. 2000; Greve et al. 2002), and produced successive and strong starbursts in the center region (e.g. Rieke et al. 1980; Förster Schreiber et al. 2001; de Grijs et al. 2001; Smith et al. 2007). Despite this encounter, on deep images and photometric tracings (e.g. Devine & Bally 1999; Ohyama et al. 2002; Mayya et al. 2005; Ichikawa et al. 1995) the nearly edge-on stellar body of M 82 extends ~10 kpc and ~3 kpc along the major and minor axes, respectively, with a surprisingly regular IR light distribution of the stars, with no warps (Davidge 2008) and tidal extensions seen in H I and CO. Rotation velocity studies of the ionized gas and stars at optical and near-IR wavelengths extend along the major axis only to ~120−160″ (~2−3 kpc)[1] from the center so that the rotation of the intermediate and outer regions of M 82 is poorly known, while outside the nuclear region the H I and CO gas shows a highly disturbed distribution and motion (Yun et al. 1993, 1994; Brouillet et al. 1991; Taylor et al. 2001; Walter et al. 2002) that may not be representative of the post-encounter bulge and disk.

Depending on the wavelength of observation and on whether gas or stars are observed, M 82's radial velocities plotted in a p–v diagram may not display a smooth curve, with a steep increase at the center and a more or less flat outer part. We discuss the apparent velocity reversal of gas and stars seen at ~50−70″ (0.9−1.2 kpc) on either side of the center and outside the bar. Although the velocity reversal is seen in earlier observations (e.g. McKeith et al. 1993; Shopbell & Bland-Hawthorn 1998; Westmoquette et al. 2009), it has escaped general attention, with the exception of the explanation by Westmoquette et al. (2009) of a different orientation of the body of the stars and the gas. We investigate the velocity reversal and the radial velocities in the outer parts of M 82 in the picture of a stellar disk with embedded corotating spiral arms, as recently outlined by Mayya et al. (2005). For this we analyze earlier and unpublished observations of radial velocities to a distance of ~±3 kpc (160″) from the center, derived from ionized gas emission lines and stellar absorption lines. We also use the inner ±200″ of a deep ^{12}CO(2–1) map, recently obtained by Weiß et al. (2009, priv. comm.).

We try to explain the radial velocity features in the context of M 82's known geometric and kinematic structure. M 82 is inclined by ~80° and seen from below (e.g. McKeith et al. 1993); the western side moves towards the observer, the eastern side moves away. Following Telesco et al. (1991), the bar is inclined by ~4° with respect to M 82's galactic plane, with the western side of the bar lying above the galactic plane. The major axis of the bar is turned out of the plane of the sky by $\omega \approx 22°$, with the eastern side more distant. H I, CO, and (near-)IR velocity observations have revealed the bar's x_1-orbits, between ~±30″, and the inner, perpendicular x_2-orbits, between ~±10″ (e.g. Wills et al. 2000; Achtermann & Lacy 1995; Greve et al. 2002). Mayya et al. (2005; see also Ichikawa et al. 1995) used IR images to derive a stellar disk of ~50″ scale length and two trailing spiral arms starting at right angles to the eastern and western extremes of the bar. However, M 82's spiral arms need not be regular structures, as shown schematically by Mayya et al. (2005, their Fig. 5), but may contain a significant degree of irregularity and asymmetry, similar to what is seen in the much larger barred galaxy NGC 4151 (Mundell et al. 1999). It will be difficult to

[1] At M 82's distance of 3.6 Mpc (Freedman et al. 1994; Sakai & Madore 1999), 1″ corresponds to 17.5 pc. All radial velocities quoted here are relative to M 82's systemic velocity of 200 km s^{-1}. We made no corrections for M 82's nearly edge-on inclination of ~80°.

find out the actual situation in this dusty edge-on galaxy. In contrast to the regular stellar bar and stellar disk, the molecular gas and ionized gas have rather irregular distributions, at visible and blue wavelengths for some part a deception because of patchy extinction across the galaxy.

2. Optical and near-IR observations

Several radio, near-IR, visible, and blue wavelength emission and absorption lines can be used for measuring radial velocities in M 82 (Table A.1). The radio emission lines probe the interstellar medium (ISM), while the optical emission lines originate in ionized gas, either located in M 82's starburst region or in H II regions distributed along spiral arms. The optical absorption lines originate in stellar atmospheres (broad lines) and in the ISM (Ca II, NaD, narrow lines). The line-of-sight superposition of gas, stellar, and ISM emission and absorption lines of the same atomic species may lead to confused spectra. The wavelength of a line determines the depth of observation in the dusty galaxy M 82.

2.1. The earlier and unpublished optical observations

In order to eventually investigate the off-axis kinematics, in 1990 we obtained long-slit spectra of Hα, [N II], and [S II] along and parallel to M 82's major axis with the 4.2 m WHT of the RGO on La Palma. The central spectrum is through the 2 μm center at $9^h51^m43.6^s$, 69°55′00″ (1950; Lester et al. 1990). The other spectra are at 5″ N (87 pc N; A), 2″ N (35 pc N; B), on-axis (C), 2″ S (35 pc S; D) and 7″ S (122 pc S; E), shown in Fig. 3. All spectra were taken at position angle 65°. The exposure times were 1000 s to 1800 s, which allows us to detect faint emission to ∼±120″ distance from the center. The seeing was 0.8″ to 1″, and the pixel spacing on the velocity axis 0.74 Å or 35 km s^{-1}. We derived radial velocities from single Gaussian profile fits to the unblended [N II] 6583 Å and [S II] 6716 Å emission lines (see Sect. 5.1).

We combined these data with radial velocities that we published earlier (McKeith et al. 1993; Greve et al. 2002; abbreviated McK93 and GWNP). We used in addition other radial velocity data at near-IR and visible wavelengths (Westmoquette et al. 2009; Whitmore et al. 1984) and data of stellar clusters (Konstantopoulos et al. 2009) and planetary nebulae (Johnson et al. 2009).

A summary of the observations of gas emission lines and stellar absorption lines is given in Fig. 1, as a function of the wavelength of observation from near-IR to blue. Globally, the near-IR wavelengths probe the central region, or even beyond, while the blue wavelengths probe the near-side outer regions of M 82. However, M 82's interstellar medium is not a homogeneous screen; it is partially transparent through locally lower dust contents and "windows" so that the higher radial velocities of the bar region are also seen at blue wavelengths (see Figs. 5 and 6 in McK93).

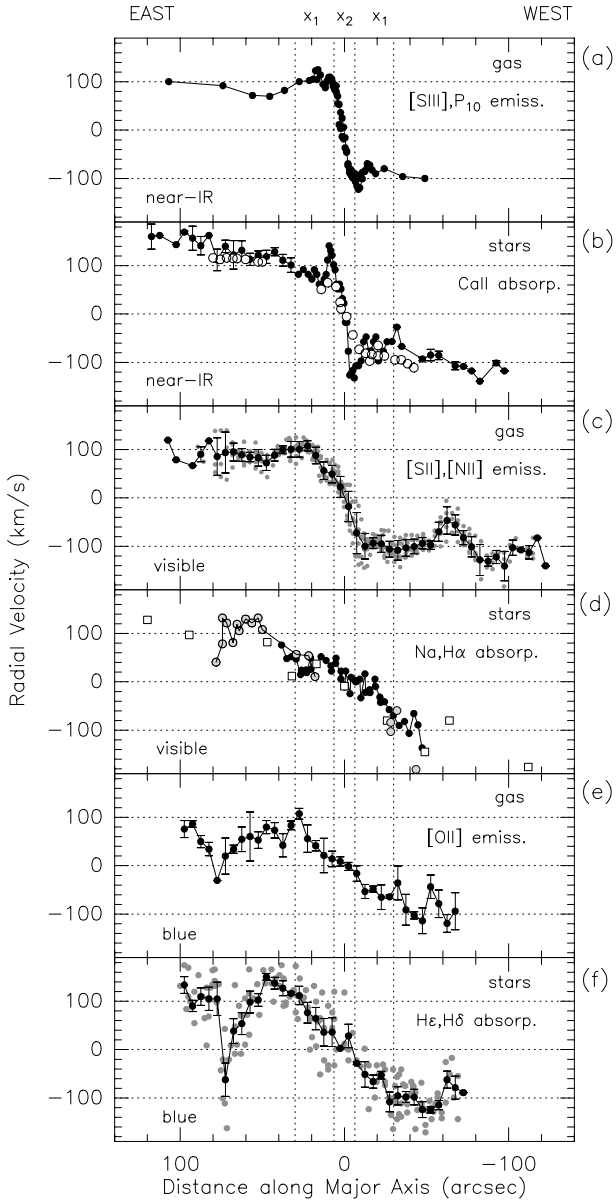

Fig. 1. Position-velocity diagram along M 82's major axis showing the motion of gas and stars; the vertical dashed lines indicate the extent of the bar (x_2 and x_1-orbits). At the top: measurements at near-IR wavelengths, which probe the center region. At the bottom: measurements at blue wavelengths, which probe the more outer regions. **a)** From McK93. **b)** Black dots: from GWNP (10″ bins); open circles: stellar Ca II measurements by Westmoquette et al. (2009). **c)** Black dots: average (5″ bins) of [SII], [NII] emission lines from Fig. 3, A–E, simulating a slit of ∼ ±7″ width; gray dots: individual measurements. **d)** Black dots: Na D measurements by Saito et al. (1984); connected gray open circles: Hα absorption line (component C4) measurement by Westmoquette et al. (2009); open squares: absorption line data from Mayall (1960). **e)**, **f)** From McK93; **f)** gray dots: individual measurements.

2.2. p–v diagrams from near-IR to blue wavelengths

The *near-IR* stellar Ca II absorption lines (8662, 8542, 8498 Å) show the velocities of the x_1 and x_2-orbits of the bar within ∼±30″ distance from the center, and a rather flat radial velocity curve beyond the bar (Fig. 1b, and GWNP). The same velocity structure of the x_2-orbits, though with higher peak velocities, is seen in the unobscured [Ne II] 12.8 μm emission line (Achtermann & Lacy 1995, see GWNP for a comparison with the stellar Ca II lines) from which it follows that there is little *average* obscuration at near-IR wavelengths so that the center region within 5 to 10″ (50 to 150 pc) distance can be seen. The recent measurement of the near-IR stellar Ca II absorption lines by Westmoquette et al. (2009) agrees with our more extended data (Fig. 1b), but the high velocities of the x_2-orbits

are not seen in their observation[2]. As also noticed by Davidge (2008), the flat or gradually increasing stellar radial velocity curve shown in Fig. 1b may contradict the declining H I and CO velocities derived by Sofue (1998), although the spatial coverage of the near-IR observation is too small to arrive at a firm conclusion. At near-IR wavelengths (Fig. 1a), the [S III] (9069 Å) and P_{10} (9015 Å) ionized gas emission lines show the velocity features of the bar; however, spraying (Athanassoula 1992; Downes et al. 1996; Wills et al. 2000, GWNP) and shocks seem to blur the clear signature of the x_2-orbits (peaks). The ionized gas outside the bar shows a flat radial velocity curve on the eastern side, although there are only a few measurements.

At *visible* wavelengths, the unblended [N II] and [S II] ionized gas emission lines show the velocities of the x_2 and x_1-orbits more or less clearly (Fig. 3). However, the outstanding feature seen in these lines is a velocity reversal of nearly 100 km s^{-1} at ~50−70″ (1−1.2 kpc) west, which extends over ~15″ (~250 pc). Farther out, the radial velocity again returns to approximately −120 km s^{-1}, as it was near the edge of the bar (at ~30″) and as measured in the near-IR stellar Ca II absorption lines (Fig. 1b). The velocity reversal at ~60″ west also appears in the Hα emission line data of McK93, Shopbell & Bland-Hawthorn (1998), and Westmoquette et al. (2009). At ~70″ east, the Westmoquette et al. (2009) Hα emission line measurement (component C1) shows very low radial velocities at a few positions, however, these few data points do not seem to show a feature like the velocity reversal seen on the western side (Figs. 1c, 3). We hesitate to use Hα emission line data because they are influenced by underlying stellar absorption (for relative line strengths see Götz et al. 1990). In our [N II] and [S II] observations (Figs. 1c, 2, 3), there is no indication of a deep velocity reversal on the eastern side.

It is difficult to measure radial velocities of stars from absorption lines at *visible* and *blue* wavelengths. The stellar Na D (5890, 5896 Å) and Ca II H & K (3933, 3968 Å) absorption lines may be contaminated by interstellar absorption in M 82, and the stellar Balmer[3] absorption lines may be partially filled by line-of-sight Balmer ionized gas emission lines (Figs. 5 and 6 in McK93). The stellar Na D absorption line observations published by Saito et al. (1984), reproduced in Fig. 1d, and the other observations at blue wavelengths (Figs. 1e, f) do not reach the center region since the velocity signature of the bar is not seen. The Na D absorption line velocities published by Konstantopoulos et al. (2009) and Götz et al. (1990; taken at ~10″ N off-axis slit position) show a large scatter and on average lower radial velocities compared to the data of Saito et al. The radial velocities of the stellar Hα absorption line (component C4) determined by Westmoquette (2009, their Fig. 20), and shown in Fig. 1d, suggest that a velocity reversal may occur at ~80″ (1.4 kpc) east, but the spatial coverage is insufficient for a clear picture. The Hα and Na D absorption line data of Mayall (1960), shifted to the current systemic velocity of 200 km s^{-1} (see Burbidge et al. 1964, for a discussion of the systemic velocity used at that time), are inserted in Fig. 1d. The measurements indicate radial velocities of ~120−180 km s^{-1} at ~±120″ distance.

Because of the higher extinction at *blue* wavelengths, the ionized gas measured in the [O II] 3727 Å emission line (Fig. 1e) and the stars measured in the Hϵ 3970 Å and Hδ 4102 Å absorption lines (Fig. 1f) do not reach the center. Both lines show a deep velocity reversal at ~70−80″ (1.3 kpc) east, i.e. at approximately the same distance as the velocity reversal in the west. The velocity reversal extends over ~15″ (~250 pc). Although for the blue emission and absorption lines there is some indication of a velocity reversal on the western side, the spatial coverage is insufficient to reveal a clear picture.

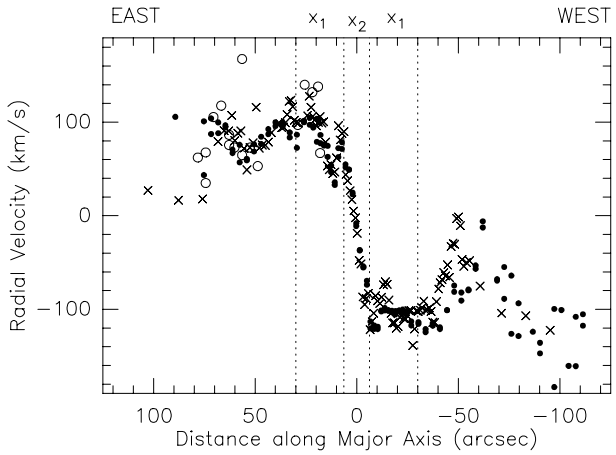

Fig. 2. Position-velocity diagram derived from visible emission lines. Black dots: [S II] emission lines measured along slit position D (Fig. 3); crosses: major axis [N II] emission line data from Castles et al. (1991); open circles: Hα C1 emission line data from Westmoquette et al. (2009).

2.3. Visible line velocity reversal on the eastern side

Although the observation at blue wavelengths shows a velocity reversal of gas and stars at ~70−80″ east (Fig. 1e, f), the absence at this position of a deep velocity reversal at visible wavelengths ([S II], [N II], Hα) is a puzzle. However, in some spectra there are indications of a weak velocity reversal at ~50″ east, as illustrated in Fig. 2. The Hα C1 emission line data of Westmoquette et al. (2009) seem to follow this reversal, although the few low Hα C1 and [N II] velocities between ~70 and 100″ east are peculiar in this picture. It is unclear why the peaks of the [N II] and [S II] line reversals occur at different positions in the west, since this is not seen in Figs. 1c and 3.

2.4. p–v diagrams parallel to the major axis

The p–v diagrams of the visible, unblended [N II] and [S II] emission lines for directions parallel to the major axis are shown in Fig. 3. The velocity feature of the bar is more or less clearly seen. The velocity reversal on the western side is seen throughout several arcsecs of the disk (~ ±2−5″ or ±40−80 pc); however, the [S II] and [N II] lines do not show the deep velocity reversal on the eastern side. The radial velocity beyond ~±80″ is rather constant and approximately ±100 km s^{-1}.

2.5. Other optical observations

We searched the literature for other observations that may indicate the velocity reversal and the shape of the radial velocity curve beyond the bar and starburst region. We found little relevant information. Most observations concentrate on the intense emission from the starburst/bar region, rather than on the more

[2] Westmoquette's et al. (2009) near-IR Ca II line radial velocity curve corresponds to a 7″ wide "pseudo"-slit contructed from four regions observed with the WIYN Integral Field Unit spectrograph, while in our observations the slit width is ~2″.

[3] And stellar Paschen absorption lines.

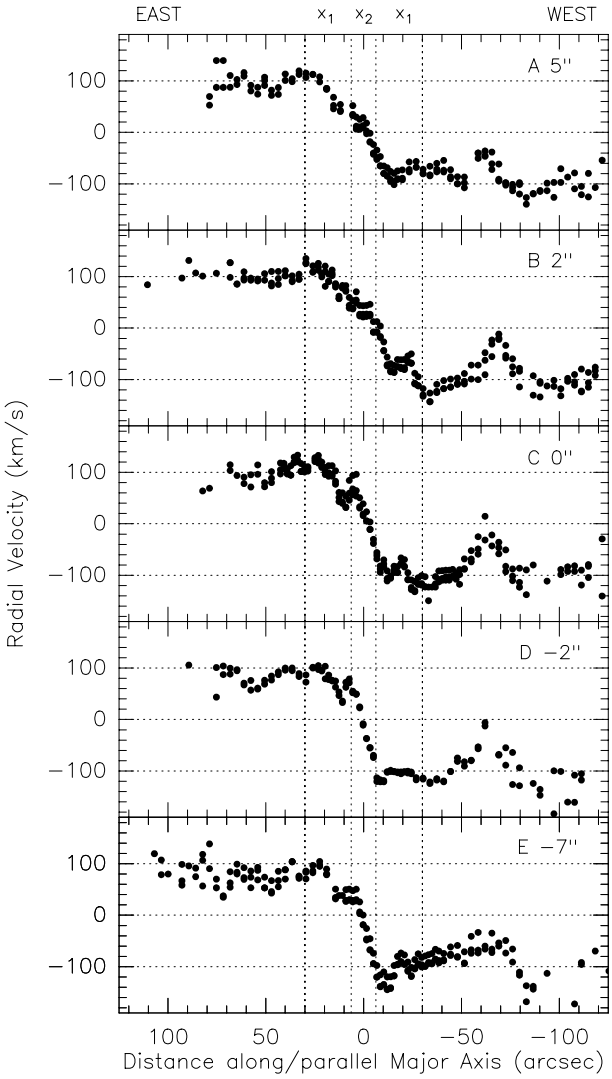

Fig. 3. Position-velocity diagram of visible [S II] and [N II] emission lines measured along and parallel to M 82's major axis as indicated. A, B: north; D, E: south.

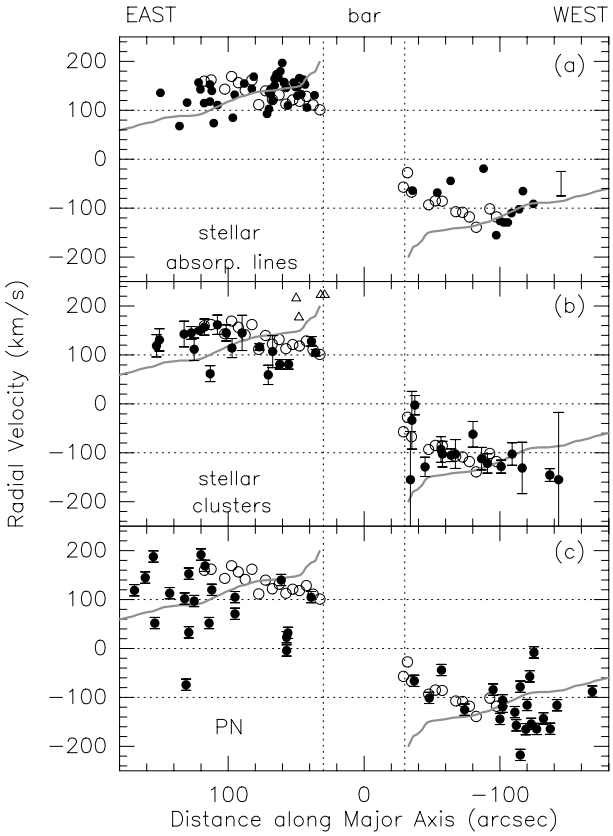

Fig. 4. a) Radial velocities of stellar absorption lines in the wavelength region 4700–5450 Å measured by Whitmore et al. (1984): black dots. The bar is the 1σ error of their data. In all panels, the open circles are the radial velocities of the near-IR stellar Ca II absorption lines shown in Fig. 1b; the continuous lines present the CO radial velocities published by Sofue (1998). **b)** radial velocities of stellar clusters (within $|z| \lesssim 500$ pc) from Konstantopoulos et al. (2009): black dots, triangles: cluster Nos. 108, 112, 2, 125, 126 with a high radial velocity, seen in the direction of complex B. **c)** radial velocities of planetary nebulae (within $|z| \lesssim 500$ pc) from Johnson et al. (2009): black dots.

difficult observation of the much weaker emission from M 82's outer region.

Whitmore et al. (1984) used stellar absorption lines at 4700–5450 Å for radial velocity measurements approximately along the major axis, in order to obtain a clearer picture of the rotation than from the "disordered velocity field of the excited gas". The radial velocities outside the bar are shown in Fig. 4a, together with the stellar radial velocities measured in the near-IR Ca II absorption lines (Fig. 1b). Both measurements seem to agree, at least on the eastern side. There is a hint of the velocity reversal at ∼70″ east, better seen in Fig. 5 of Whitmore et al. (NE central scan). The radial velocity is $\sim\pm100-150\,\mathrm{km\,s^{-1}}$ at ±100–140″ distance.

Figure 4b shows the radial velocities of stellar clusters measured by Konstantopoulos et al. (2009) up to ∼±160″ distance, using spectral templates at 4000–6000 Å. The clusters selected for the figure are located outside the bar and within ∼500 pc above and below the galactic plane. Figure 3 suggests that the velocity reversal is confined to a thin layer around the galactic plane so that the reversal is not seen in these data. Globally, the cluster radial velocities follow and extend the radial velocities measured in the near-IR stellar Ca II absorption lines (Fig. 1b). The radial velocity is $\sim\pm140-160\,\mathrm{km\,s^{-1}}$ at ∼±100–160″ distance. There are four clusters (Nos. 108, 112.2, 125, 126, between 30 to 50″ east) with radial velocities 60 to 100 $\mathrm{km\,s^{-1}}$ higher than measured in the near-IR stellar Ca II absorption lines. These clusters are located in the direction of the stellar complex B (O'Connell et al. 1995). Konstantopolous et al. (2009) assume that there is a "window" in the direction of complex B so that here the clusters are seen at greater depths, with correspondingly higher radial velocities. The spectra of Figs. 1–3, however, do not show any higher radial velocities in this direction.

The radial velocities of planetary nebulae within ∼±500 pc distance from the galactic plane are taken from Johnson et al. (2009) and shown in Fig. 4c. The scatter of the velocities is large. Nevertheless, the envelope of the maximum radial velocities seems to agree with the radial velocities measured in the near-IR stellar Ca II absorption line (Fig. 1b). The maximum radial velocity is close to $200\,\mathrm{km\,s^{-1}}$ at ∼±120–140″ distance.

3. Radial velocities measured in CO

In the bar region, there is agreement between the motion of the CO gas, H I gas (Wills et al. 2000), the ionized gas and the stars (Figs. 1a, b; GWNP) because the bar potential acts in an identical way on the stars and the gas. The CO observations outside

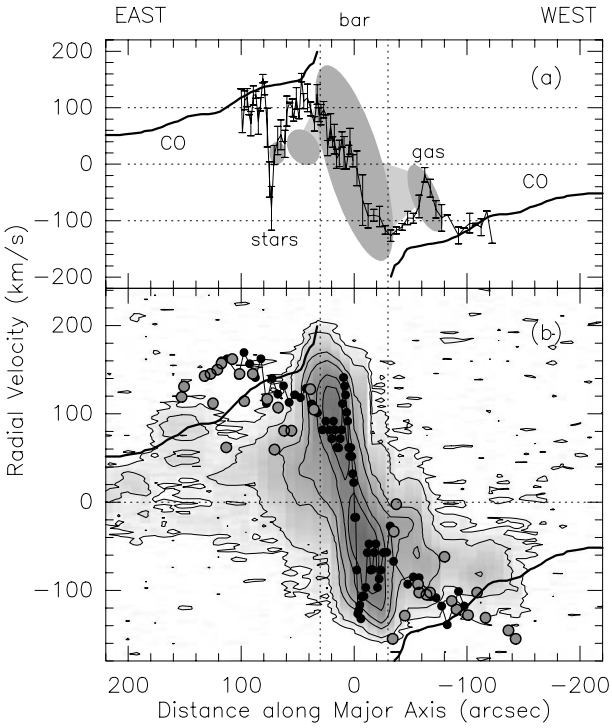

Fig. 5. a) Schematic representation of measured ^{12}CO(1–0) radial velocities (from Walter et al. 2002, interferometer measurements). Overlaid on the eastern side: velocity reversal observed in stellar motions (Fig. 1f); western side: velocity reversal observed in [S II], [N II] emission lines (Fig. 1c). **b)** ^{12}CO (2–1) radial velocities (contours at 0.03, 0.1, 0.5, 1, 2.5, 4, and 10 K). Overlaid are radial velocities of stars: black dots (Fig. 1b) and of stellar clusters: open circles (from Konstantopoulos et al. 2009, and Fig. 4b). The line in **a)** and **b)** is the smooth ^{12}CO(2–1) radial velocity curve published by Sofue (1998). The IRAM 30-m telescope CO data shown in **b)** are from Weiß et al. (2009, priv. comm.) [HERA 9-channel receiver, 11″ beam width].

the bar are taken from Sofue (1998), Seaquist & Clark (2001), Walter et al. (2002), and Weiß et al. (2009, priv. comm.).

Sofue (1998) analyzed CO and H I data up to ∼±4′ (∼±4.2 kpc) distance from the center and constructed a smooth rotation curve representative for the rotation at the western and eastern side. There is no sign of the velocity reversal in the smooth CO and H I curve. There is some indication of the reversal on the western side in the interferometer CO study by Seaquist & Clark (2001, their Fig. 5). Clear evidence of velocity reversal at ∼50″ west and between 30 to 60″ east is seen in the ^{12}CO (1–0) interferometer observation along the major axis at position angle 75° through the center by Walter et al. (2002, their Fig. 5), which is schematically reproduced in Fig. 5a. The observations of Fig. 5 show an asymmetric CO distribution with less CO on the eastern side, as seen earlier by Young & Scoville (1984) and Sofue (1992, 1998). The ^{12}CO (2−1) radial velocity curve published by Sofue (1998), derived from the envelope tracing method applied to single-dish observations (Sofue 1996, 1997), is inserted in Fig. 5 as a solid line. This CO (and H I) radial velocity curve shows a gradual decline from ∼200 km s^{-1} at the center to ∼50 km s^{-1} at ∼3 kpc (∼3′) distance. According to Sofue, this velocity-distance dependence indicates a Keplerian motion around a centrally concentrated mass, assumed to be the remains of the bulge and stellar disk of the original M 82-galaxy.

The interferometer CO observation (Fig. 5a) does not contain the diffuse CO emission. Figure 5b shows the radial velocities in ^{12}CO(2–1) along the major axis at position angle 65° through the center measured by Weiß et al. (2009, priv. comm.) with the HERA 9-channel receiver on the IRAM 30-m telescope (Schuster et al. 2004). Again, the asymmetric spatial distribution and asymmetric velocity distribution of the CO is evident. The even more extended and weaker CO, outside the map of Fig. 5b, warps away from the galactic plane, on the eastern and western sides (e.g. Walter et al. 2002, their Figs. 1 and 2).

In essence, Fig. 5b is similar to the CO map published by Sofue (1998). On the western side, outside the bar, there is a wide range in radial velocity from ∼−130 km s^{-1} to ∼−50 km s^{-1}. We assume that the high radial velocities of ∼−130 km s^{-1}, between 30″ to 140″ west (appoximately of 2 kpc extent), is CO seen at tangential radial distances[4], while the CO with lower radial velocity is located farther out in the galaxy. This interpretation is supported by similarly high radial velocities of the stars and stellar clusters seen at these distances (Fig. 5b). On the eastern side, outside the bar, the radial velocities are significantly lower than the radial velocities seen in the near-IR stellar Ca II lines and stellar cluster motion.

4. The radial velocity of the stellar disk

Figure 6 shows the bar and the trailing spiral arms (Mayya et al. 2005), with M 82 seen from above (north) as in the picture of the bar shown by GWNP (their Fig. 3). The gray background in Fig. 6a is the stellar disk of ∼50″ scale length (Ichikawa et al. 1995; Mayya et al. 2005). Since the near-IR stellar Ca II absorption lines trace the center of the bar (Fig. 1b), we can assume that these lines trace outside the bar also the inner parts of the galaxy. The radial velocities measured in the near-IR stellar Ca II absorption lines are those near tangential points of the disk stellar orbits[4]; they display a flat or even increasing radial velocity curve, with no velocity reversal and no indication of spiral arms. The smoothness of the radial velocity curve (Figs. 1b, 6b) indicates that at near-IR wavelengths there is little line-of-sight interstellar extinction, and that the intervening spiral arms are transparent enough so that the tangential radial velocities are observed.

5. Search for the origin of the velocity reversal

5.1. Velocity reversal and multiple emission line components

The profiles of emission lines can be narrow, approaching the spectral resolution as judged from the shape of a sky emission line. They also can be broad or consist of individual emission line components that are more or less well resolved. Westmoquette et al. (2009) distinguish three components, namely component C1 of 90−116 km s^{-1} *FWHM*, component C2 of 212−224 km s^{-1} *FWHM*, and component C3 of 68−103 km s^{-1} *FWHM*. They provide several illustrations of the components (their Fig. 4); however, for certain cases there is ambiguity in the way the components were chosen and under which astrophysical necessity. The prominent line splitting seen in their Figs. 4c, f is observed at ∼10″ south of the major axis. These profiles are similar to those observed by Götz et al. (1990) at ∼10″ north, which were interpreted as already showing the minor axis outflow.

We analyzed our observations with single-component Gaussian profiles, with free parameters the center wavelength, the line width, and the peak intensity. Figure 7 illustrates this

[4] Where the orbital velocity vector is in the direction of the line-of-sight.

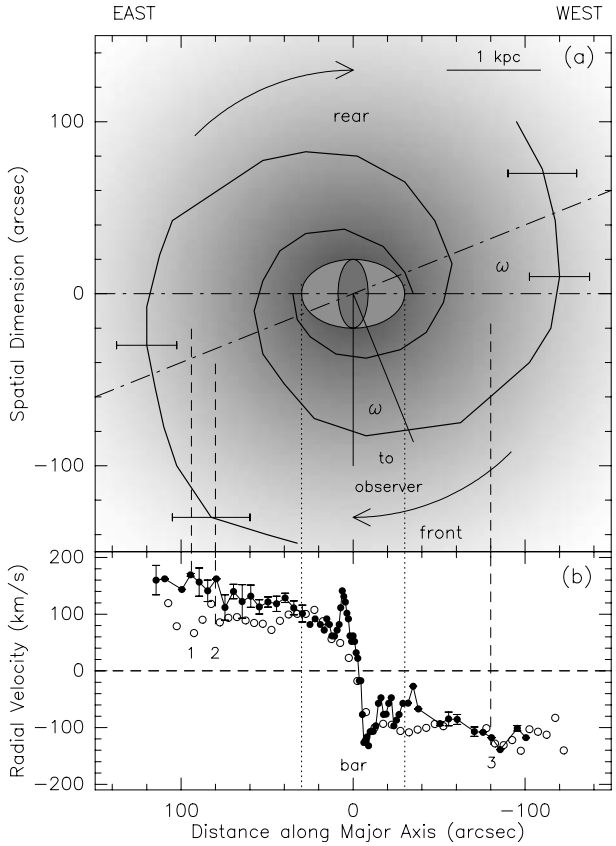

Fig. 6. Schematic view of M 82's structure and radial velocities. **a)** M 82 seen from the top (north), showing the bar, the stellar disk (gray background) and the trailing spiral arms (from Mayya et al. 2005). The spiral arms may have a width as schematically indicated by the horizontal bars. The arrows indicate the rotation. The bar, hence also the spiral arms, may be viewed under the angle $\omega \approx 22°$ so that the dashed-dotted line is the plane of the sky. **b)** Black dots: radial velocities of the near-IR stellar Ca II absorption lines (Fig. 1b) tracing the stellar disk; open circles: radial velocities of the visible ionized gas [N II], [S II] lines (Fig. 1c), with the velocity reversal at ∼70″ west omitted. The dashed lines 1, 2, 3, for example, indicate approximately the region where the radial velocities of the Ca II lines are measured.

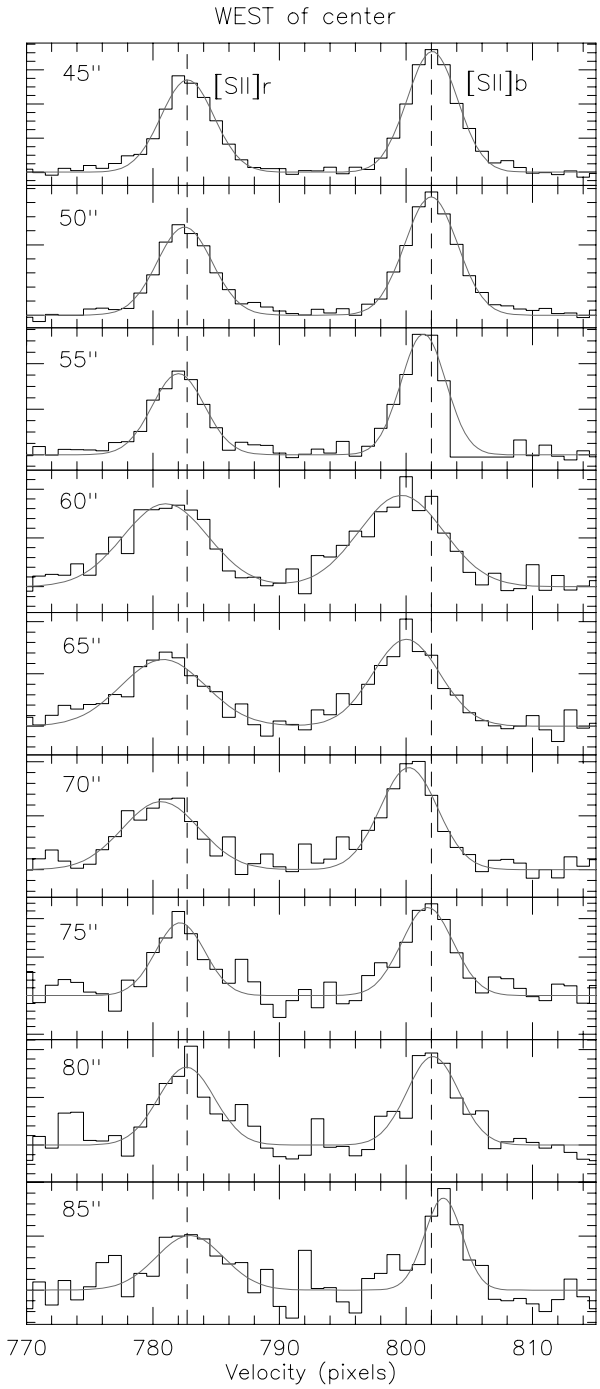

Fig. 7. [S II] 6716 Å (b) and 6731 Å (r) lines and single Gaussian profiles fits to the spectrogram C of Fig. 3. The positions (west) of the profiles are indicated. Two pixels (one tick mark) is 70 km s^{-1}. The vertical dashed lines illustrate the velocity shift; the reversal occurs near 60−70″. From 45 to 85″, the line intensity decreases by a facter of ∼10, with a corresponding increase in noise. (The *FWHM* of a weak skyline (near Hα) is 2.5 pixels.)

procedure for the unblended [S II] 6716,6731 Å emission lines observed on the western side of the center where the velocity reversal is strong (Figs. 1−3).

Since, when present, the broad line component C2 seems to be weaker than the narrow components C1 and C3, and since the blue stellar absorption lines (Fig. 1f) and blue [O II] gas emission lines (Fig. 1e) do not show evident multiple components, we hesitate to explain the velocity reversal as due to a multiple-component line structure. At distances from the major axis greater than 10−15″, a multi-component line structure may come partially from superposition of the minor axis outflow with line splitting (e.g. Greve 2004).

5.2. Velocity reversal and (kinematic) substructures

M 82 contains several substructures in the bar region and outside the bar that may have different orientations with respect to a global major axis and which in addition may have a different kinematic behavior. The Telesco et al. (1991, their Fig. 12) investigation shows clearly that, inside the bar region (∼±30″ distance), the distribution of stars (2.2 μ radiation) and molecular gas (CO, see also Shen et al. 1995; and Neininger et al. 1998) is different, even though the stellar bar potential is the dominent gravitational force. Despite different spatial distributions in the bar region, with apparently different "major" axes, nevertheless the radial velocities of H I and CO (Wills et al. 2000), objects with radio recombination line emission (Rodriguez-Rico et al. 2004), supernova remnants (Wills et al. 2000), and stars (GWNP) are very similar. The bar itself is inclined by ∼4° to the material at large radial distances (Telesco et al. 1991). Outside

the bar, at radial distances greater than ∼±40−60″, Ichikawa et al. (1995, their Fig. 8) suggest that the distribution of the stars (position angle and b/a ratio) is different from the stars in the bar region. As the investigations by Walter et al. (2002) and Weiß et al. (2005) show, at these radial distances the CO distribution on the western side warps to the south (S_1), while on the eastern side the CO distribution warps to the north (S_2) and to the east and south (S_4 and S_3). The velocity reversal occurs near these regions of gas warping, where the molecular gas density is a factor of ∼10 lower than in the center region. Although some spatial coincidence exists, it is unclear whether the velocity reversal is associated with these morphological features.

Westmoquette et al. (2009) attribute the velocity reversal to a ∼12° difference in position angle of the rotation axes of the gas and the stars. They state that this difference in alignment extends over the inner 2 kpc, that is ∼±60″. At the ∼±50−70″ distance of the reversal, a 12° position angle difference would bring either the plane of the stars or the plane of the gas approximately 250 pc above, or below, one or the other plane. This distance is, on the one hand, large compared with the thickness of the layer in which the reversal apparently occurs (Fig. 3), and, on the other hand, seems to contradict the comparative study of the distribution of stars and gas made by Walter et al. (2002, their Fig. 2). The asymmetric reversal between the eastern and western sides measured in the long-slit observation of the [N II] and [S II] lines shown in Fig. 2 may favor Westmoquette et al. explanation. However, the fact that – at least on the eastern side – the gas (Fig. 1e) *and* the stars (Fig. 1f) show the strong velocity reversal at the same radial position is not easily reconciled with their explanation.

5.3. The velocity reversal and M 82's spiral arms

Velocity reversals have been observed in barred galaxies (Bettoni et al. 1988, and references therein), in some cases due to retrograde x_4-orbits (Sellwood & Wilkinson 1993). For these unusual galaxies the reversal occurs, however, *inside* the bar, not *outside* as in M 82. We thus believe that in M 82 the velocity reversal is not a retrograde motion. We investigate whether the reversal is a projection effect of the two-armed trailing spiral, as schematically shown in Fig. 8.

For a model calculation of the spiral arm velocities seen projected along the spectrograph slit, we assume that (*a*) the spiral arms as derived by Mayya et al. (2005) start at right angles at the extremes of the bar; (*b*) they follow within the observed ∼30 to 160″ radial distance the constant rotation of the stellar disk of $v(r) = v \approx 140{-}160\,\mathrm{km\,s^{-1}}$ (Figs. 1b, 4); (*c*) the spiral arms contain stellar clusters, H II regions, and molecular gas with corresponding emission and absorption lines, while the interarm regions are essentially empty; (*d*) the observations at visible and blue wavelengths, at which the velocity reversal is seen, reach sections of the spiral arms that are located in front of the center. The spiral arms beyond the center are mostly hidden behind dust. The correspondingly predicted projected radial velocities of the eastern and western spiral arms (E-arm, W-arm) are shown in Fig. 8b.

According to this model, the high radial velocities of $\sim 120{-}140\,\mathrm{km\,s^{-1}}$ occur in the tangential directions of the spiral arms, that is, at the positions E_1, E_2, E_3 and W_1, W_2, W_3 of the eastern and western spiral arms, respectively. A part of the apparent velocity reversal may come from spiral arm material approximately located at the position RE in the east and RW in the west. However, as Fig. 8b illustrates, the spiral arm material at RW and RE cannot have the observed low radial velocities of the reversal of $\sim -40\,\mathrm{km\,s^{-1}}$. Material farther inside along this line-of-sight has a higher velocity, while only material much farther outside may reach the low radial velocities.

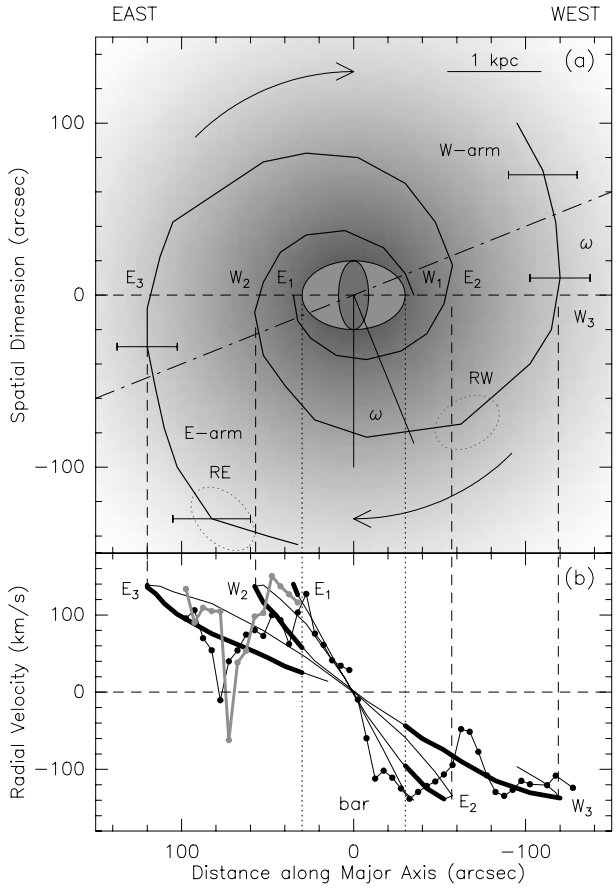

Fig. 8. Schematic view of M 82's structure **a)**, as explained in Fig. 6. **b)** p–v diagram showing the radial velocities of the spiral arms projected along the spectrograph slit. Thin lines: line-of-sight radial velocities of the eastern and western spiral arms; heavy lines: line-of-sight radial velocities of the eastern and western spiral arm sections at the *front* of the galaxy (i.e. either in front of the dashed line or the dashed-dotted line). Dots on western side: ionized gas [S II], [N II] emission lines (Fig. 1c); black dots on eastern side: blue [O II] ionized gas emission line (Fig. 1e), gray dots on eastern side: blue Hϵ, Hδ stellar absorption lines (Fig. 1f).

We repeated the calculation of Fig. 8 using the declining CO radial velocity curve published by Sofue (1998; Fig. 5), which we assume the spiral arms follow. Compared to the uncertainties of the model and the scatter in the observations, the difference to Fig. 8b is too small to draw a conclusion about the shape of the radial velocity curve.

5.4. The stellar disk-spiral arm model and inconsistencies

When using the spectroscopically easily accessible [N II] and [S II] ionized gas emission lines for determining M 82's radial velocities, as frequently done in the past (e.g. Burbidge et al. 1964; Heckathorn 1972; O'Connell & Mangano 1978; Götz et al. 1990; McK93, Westmoquette et al. 2009), a major axis p–v diagram is obtained as shown in the Figs. 1c, 2, and 3. The radial velocity curve is asymmetric, with a strong velocity reversal on the western side, which escapes easy interpretation when having only these data.

When adding the observations of the near-IR stellar Ca II absorption lines (Fig. 1b) and the near-IR [S III] and P_{10} ionized gas emission lines (Fig. 1a) to the [N II] and [S II] line data, two features can be explained, while the velocity reversal remains unexplained. At M 82's center, the velocities of the near-IR stellar Ca II absorption lines agree with those of the bar measured in H I and CO, along and parallel to the major axis (Wills et al. 2000), from which it follows that the gas and the stars of the bar rotate in the same way. Outside the bar, the near-IR stellar Ca II absorption lines show a flat radial velocity curve, on the eastern and western sides, which we assume represent the rotation of the stellar disk.

The addition of radial velocity measurements of the visible Hα and Na D stellar absorption lines (Fig. 1d) does not help tracing the origin of the velocity reversal. The Balmer lines and Na D lines may be severely blended, either by ionized gas emission or interstellar absorption (Table A.1), thus falsifying the radial velocity measurement.

When adding the observations at blue wavelengths it is important to recognize that because of extinction the blue lines originate only in the near-side outer regions of the galaxy, and that the spatial coverage in the west is incomplete in our and other observations. On the eastern side, a deep velocity reversal is measured in the [O II] ionized gas emission line (Fig. 1e) and the stellar H ϵ, H δ absorption lines (Fig. 1f).

Information on the location of the material with velocity reversal is drawn from the following facts

- Since the velocity reversal occurs on the western *and* eastern sides at approximately the same radial distance from the center (~±50−70″), outside the bar, it is unlikely that heavy local extinction causes the velocity reversal. The velocity reversal appears to the west of the stellar G-complex and to the east of the stellar B-complex (O'Connell & Mangano 1978).
- The velocity reversal is *not* seen in the near-IR Ca II absorption lines of the stellar disk, neither on the western nor on the eastern side, from which it follows that the material with velocity reversal is not directly associated with the "smooth" stellar disk. Additional information that the stars with velocity reversal are different from the stars of the disk is obtained from comparing the *near-IR* stellar Ca II absorption line velocities, shown in Fig. 1b, with the *blue* stellar Ca II K (and H) absorption line velocities (McK93), both shown in Fig. 9. The stars seen without velocity reversal in the blue stellar Ca II absorption line are stars of the stellar disk, as evident from their radial velocity curve. The blue stellar Ca II K line and Hϵ, Hδ lines have a lower velocity gradient (Figs. 1e, f), indicating that the corresponding stars are located well in front of the center (McK93).
- The model calculation displayed in Fig. 8 reproduces only a part of the observed velocity features, but not the full amount of the reversal and not the negative velocities. A substantial part of the gas and stars with velocity reversal must be located outside the spiral arms.

The CO (and H I) radial velocities reveal a more complicated structure. At M 82's center, the bar potential governs the distribution and motion of CO (Wills et al. 2000), while outside the bar the CO has an irregular and asymmetric distribution and motion (see Fig. 5), with warps and tidal arms (e.g. Walter et al. 2002; Taylor et al. 2001). Although the CO usually follows the spiral arms (with a high arm-interarm contrast), the CO radial velocities shown in Fig. 5 do not indicate the spiral arms, and in particular the velocity reversal. The CO with constant high radial velocities of ~−130 km s^{-1}, on the western side (Fig. 5), has

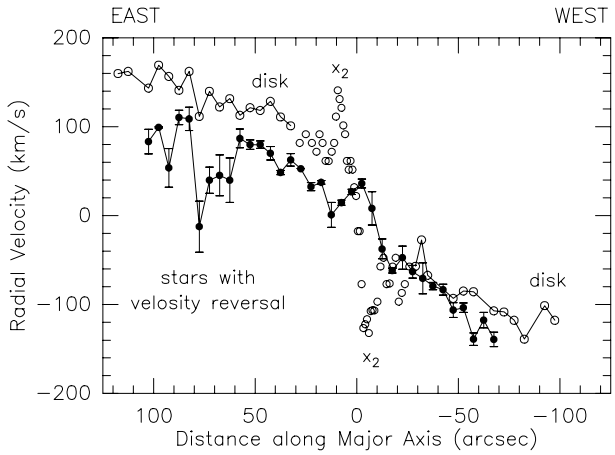

Fig. 9. Radial velocities of the stellar disk (open circles), measured in the near-IR stellar Ca II absorption lines (Fig. 1b) not showing a velocity reversal, and stars with velocity reversal (dots) measured in the blue stellar Ca II K line (from McK93).

nearly the same tangential radial velocities as observed in the near-IR stellar Ca II absorption lines. The CO with lower radial velocity is located in the front (or beyond the center) so that the velocity vector is inclined to the line-of-sight, nearly reaching a perpendicular direction. In this picture, the CO beyond the bar is distributed – though perhaps in a clumpy way – throughout a large volume of the stellar disk. As Fig. 5 shows, the distribution and motion of CO is more regular on the western side than on the eastern side (Yun et al. 1993; Walter et al. 2001).

There are some puzzling features when using the picture of a stellar disk and spiral arms. The eastern and western spiral arm, intervening in the line-of-sight, must be rather transparent since otherwise the tangential radial velocities of the bar and stellar disk could not be observed in the near-IR Ca II absorption lines. The smoothness of the near-IR Ca II radial velocity curve indicates a rather smooth distribution of extinction.

The [N II], [S II], [O II], and Balmer emission lines appear simultaneously in H II regions. These lines are strong and easily detectable. There is a contradiction, in that on the eastern side a deep velocity reversal is seen in the blue [O II] emission line (Fig. 1e) but at the same position a much shallower reversal occurs in the visible [N II] and [S II] emission lines (Fig. 3).

As shown by Figs. 1c and 2, the [N II] and [S II] ionized gas emission lines of H II regions show on the eastern and western sides beyond the region of velocity reversal a rather flat radial velocity curve, similar to the near-IR Ca II lines of the stellar disk. This feature gives the impression of an even distribution of ionized gas, hence of H II regions, throughout the stellar disk, rather than along spiral arms with empty interarm regions. This feature speaks against the assumption of very regular spiral arms/interarm regions, at least on the eastern side.

At blue wavelengths, the eastern velocity reversal seen in the [O II] ionized gas emission line (Fig. 1e) and the stellar Hϵ, Hδ (Fig. 1f) and Ca II K (McK93) absorption lines reach significant negative radial velocities. The negative velocities cannot be explained from the roration of a stellar disk with embedded corotating spiral arms.

6. Summary

Up to now, the optical and (near-)IR radial velocity observations of stars and ionized gas along and parallel to M 82's major axis are still limited to ~±160″ (~3 kpc) distance, while the radial

velocities derived from H I and CO beyond the bar may be disturbed by a warped distribution and tidal arms with irregular motions (Yun et al. 1993, 1994; Taylor et al. 2001; Walter et al. 2002). When we arrange the long-slit observations according to the wavelength of observation (Fig. 1), hence roughly according to the depth of observation in the dusty edge-on galaxy, and when we keep in mind that at certain wavelengths there may be insufficient spatial coverage, we find (a) that the near-IR stellar Ca II absorption lines show the very regular radial velocity pattern of the bar and the stellar disk, and (b) that at visible and blue wavelengths a velocity reversal, reaching $\sim$100 km s^{-1} or more, is seen in ionized gas emission lines on the western and eastern sides, and in stellar absorption lines on the eastern side. The velocity reversal is seen in the blue stellar Balmer lines (Fig. 1f) and the blue stellar Ca II lines but is *not* seen in the near-IR stellar Ca II lines (Fig. 9).

From the observations we arrive at the following conclusions.

1. Infrared images show that the stars, which contain the dominant visible part of the gravitational mass, have the regular spatial distribution of a bar[5] and a disk. The regular motion of the bar and the disk is measured in the near-IR stellar Ca II lines, close to the tangential points of the stellar orbits, with little obstruction by interstellar extinction in the otherwise dusty galaxy. Because the velocity reversal is not seen in the near-IR stellar Ca II lines, it follows that the reversal is not inherent to the disk, and that the mass of the stars with velocity reversal is probably much lower than the mass of the bar and the disk. The comparison of radial velocities measured in the near-IR and blue stellar Ca II lines provides evidence that the stars with velocity reversal are distinctly different from the stellar disk, as shown in Fig. 9.
2. The velocity reversal occurs at symmetrical positions on the eastern *and* western sides. It therefore is unlikely that the velocity reversal is an effect of local extinction. The location of the stellar and gaseous material with velocity reversal is difficult to assess. Because of enhanced extinction, the blue lines with velocity reversal ([O II] of Fig. 1e; Hϵ, Hδ of Fig. 1f) originate only in the near-side outer regions, while the visible lines with velocity reversal ([N II] and [S II] of Figs. 1c, 2, and 3) may also originate quite deep in the galaxy. This is evident from the fact that the visible lines display some of the velocity structure of the bar (Figs. 2 and 3).
3. Although Mayya & Carrasco (2009) state that M 82's spiral arms have little contrast with respect to the stellar disk and that star formation in the disk and spiral arms has stopped some 100 Myr ago, some stars and ionized gas with velocity reversal may be located in the spiral arms. Figure 8 illustrates that only a part of the velocity reversal can be explained as a velocity projection effect of the two-armed spiral, which corotates with the stellar disk. We outlined that this picture contains several inconsistencies.
4. Radio interferometer and single-dish CO measurements do not provide convincing evidence of the velocity reversal. Outside the bar, where the velocity reversal occurs, the distribution and motion of CO and H I gas is rather irregular (Fig. 5; Sofue 1998; Walter et al. 2002) and probably still under the influence of the encounter.
5. While the velocity reversal is a spectacular feature of the visible and blue radial velocity curves, it may however only be a secondary kinematic feature in an otherwise dominant velocity field of the regular stellar bar, stellar disk and halo. In this context, a tidal interaction calculation may be interesting, similar to the one by Yun (1999), but containing more structural detail *and* velocity information for M 82.

The observed near-IR flat stellar radial velocity curve, though limited in spatial extent, seems to contradict the declining radial velocity curve derived by Sofue (1998) from CO and H I measurements. However, the opinion that the CO and H I at large radial distances may not yield true rotational velocities was, for instance, brought up by Whitmore et al. (1984), Davidge (2008), and Mayya & Carrasco (2009), with the authors pointing out that the true tangential velocities representing the kinematically dominant mass of the bar, bulge, and stellar disk may only be measurable in stellar absorption lines. Since the Balmer stellar absorption lines may be influenced by ionized gas Balmer emission lines, an uncontaminated measurement exploring the rotation of the outer region of the disk should be based on the near-IR stellar Ca II absorption lines or, with some reservation because of interfering interstellar absorption (Table A.1), on the blue Ca II stellar absorption lines. Observations of the blue stellar Ca II lines up to 160″ radial distance are reported by Mayya et al. (2006).

Acknowledgements. I thank D. Downes (IRAM) for many discussions of a possible explanation of the velocity observations, which showed that inconsistencies remain. A. Weiß (MPIfR) provided the CO observations used in Fig. 5. I appreciated the referee's critical comments, which rightly raised doubts on the explanation of the reversal as exclusively due to the spiral arms. The comments led to a significant revision, leaving the velocity reversal still a puzzling problem.

Appendix A

Emission and absorption lines for radial velocity studies.

Table A.1. Spectral lines for rotation studies.

Element[a]	Origin[b]	Location	Contamination
Radio			
H I*, CO*	ISM	thoughout M 82	none
near-IR			
H-Paschen	H II[c] (e)	spiral arms	stars(a)
[S III]*	H II (e)	spiral arms	none
Ca II*	stars (a)	stellar disk	none (tidal arms)
visible			
[S II]*	H II (e)	spiral arms	none
[N II]*	H II (e)	spiral arms	none
Hα	H II (e)	spiral arms	stars (a)
Hα	stars (a)	stellar disk	H II (e)
Na	stars (a)	stellar disk	ISM (a)
blue			
H-Balmer	H II (e)	spiral arms	stars (a)
H-Balmer	stars (a)	stellar disk	H II (e)
[O II]*	H II (e)	spiral arms	none
Ca II H&K	stars (a)	stellar disk	ISM (a)

Notes. [(a)] Elements and wavelength region of observation, strong, unblended lines are denoted by *. [(b)] e: emission line, a: absorption line. [(c)] H II regions excited by young stars.

References

Achtermann, J. M., & Lacy, J. H. 1995, ApJ, 439, 163
Athanassoula, E. 1992, MNRAS, 259, 345
Bettoni, D., Galletta, G., & Vallenari, A. 1988, A&A, 197, 69
Brouillet, N., Baudry, A., Combes, F., Kaufman, M., & Bash, F. 1991, A&A, 242, 35
Burbidge, E. M., Burbidge, G. R., & Rubin, V. C. 1964, ApJ, 140, 942

[5] And possibly a bulge.

Castles, J., McKeith, C. D., & Greve, A. 1991, Vist. Astron., 34, 187
Davidge, T. J. 2008, AJ, 136, 2502
de Grijs, R., O'Connell, R. W., & Gallagher, J. S. 2001, AJ, 121, 768
Devine, D., & Bally, J. 1999, ApJ, 510, 197
Förster Schreiber, N. M., Genzel, R., Lutz, D., & Kunze, D. 2001, ApJ, 552, 544
Freedman, W. L., Hughes, S. M., Madore, B. F., et al. 1994, ApJ, 427, 628
Götz, M., McKeith, C. D., Downes, D., & Greve, A. 1990, A&A, 240, 52
Greve, A. 2004, A&A, 416, 67
Greve, A., Wills, K. A., Neininger, N., & Pedlar, A. 2002, A&A, 383, 56 (GWNP)
Heckathorn, H. M. 1972, ApJ, 173, 501
Ichikawa, T., Yanagisawa, K., Itoh, N., et al. 1995, AJ, 109, 2038
Johnson, L. C., Mendez, R. H., & Teodorescu, A. M. 2009, ApJ, 607, 1138
Konstantopoulos, I. S., Bastian, N., Smith, L. J., et al. 2009, ApJ, 701, 1015
Larkin, J. E., Graham, J. R., Matthews, K., et al. 1994, ApJ, 420, 159
Lester, D. F., Carr, J. S., Joy, M., & Gaffney, N. 1990, ApJ, 352, 544
Mayall, N. U. 1960, Ann. Astrophys., 23, 344
Mayya, Y. D., & Carrasco, L. 2009, Rev. Mex. Astron. Astrofis. Conf. Ser., 37, 44
Mayya, Y. D., Carrasco, L., & Luna, A. 2005, ApJ, 628, L 33
Mayya, Y. D., Bressan, A., Carrasco, L., & Hernadez-Martinez, L. 2006, ApJ, 649, 172
McKeith, C. D., Castles, J., Greve, A., & Downes, D. 1993, A&A, 272, 98 (McK93)
Mundell, C. G., Pedlar, A., Shone, D. L., & Robinson, A. 1999, MNRAS, 304, 481
Neininger, N., Guelin, M., Klein, U., Garcia-Burillo, S., & Wielebinski, R. 1998, A&A 339, 737
O'Connell, R. W., & Mangano, J. J. 1978, ApJ, 221, 62
Ohyama, Y., Taniguchi, Y., Iye, M., et al. 2002, PASJ, 54, 891
Rieke, G. H., Lebofsky, M. J., Thompson, R. I., Low, F. J., & Tokunaga, A. T. 1980, ApJ, 238, 24
Rodriguez-Rico, C. A., Viallefond, F., Zhao, J.-H., Goss, W. M., & Anantharamaiah, K. R. 2004, ApJ, 616, 783
Saito, M., Sasaki, M., Kaneko, N., Nishimura, M., & Toyama, K. 1984, PASJ, 36, 305
Sakai, S., & Madore, B. F. 1999, ApJ, 526, 599
Schuster, K.-F., Boucher, C., Brunswig, W., et al. 2004, A&A, 423, 117
Seaquist, E. R., & Clark, J. 2001, ApJ, 552, 133
Sellwood, J. A., & Wilkinson, A. 1993, Rep. Progr. Phys., 56, 173 (STSI Reprint 707)
Shen, J., & Lo, K. Y. 1995, ApJ, 445, L 99
Shopbell, P. L., & Bland-Hawthorn, J. 1998, ApJ, 493, 129
Smith, L. J., Bastian, N., Konstantopoulos, I. S., et al. 2007, ApJ, 667, 145
Sofue, Y. 1996, ApJ, 458, 120
Sofue, Y. 1997, PASJ, 49, 17
Sofue, Y. 1998, PASJ, 50, 227
Sofue, Y., Reuter, H.-P., Krause, M., Wielebinski, R., & Nakai, N. 1992, ApJ, 395, 126
Taylor, C. L., Walter, F., & Yun, M. S. 2001, ApJ, 562, L 43
Telesco, C. M., Campins, H., Joy, M., Dietz, K., & Decher, R. 1991, ApJ, 369, 135
Walter, F., Weiß, A., & Scoville, N. 2002, ApJ, 580, L 21
Weiß, A., Walter, F., & Scoville, N. Z. 2005, A&A, 438, 533
Westmoquette, M. S., Smith, L. J., Gallagher, J. S., et al. 2009, ApJ, 696, 192
Whitmore, B. C., Rubin, V. C., & Ford, W. K. 1984, ApJ, 287, 66
Wills, K. A., Das, M., Pedlar, A., Muxlow, T. W. B., & Robinson, T. G. 2000, MNRAS, 316, 33
Young, J. S., & Scoville, N. Z. 1984, ApJ, 187, 153
Yun, M. S. 1999, in Galaxy Interactions at Low and High Redshifts, ed. J. E. Barnes, & D. B. Sanders, IAU, 81
Yun, M. S., Ho, P. T. P., & Lo, K. Y. 1993, ApJ, 411, L17
Yun, M. S., Ho, P. T. P., & Lo, K. Y. 1994, Nature, 372, 530